in oil pipeline systems. *AIChE J.* 39(8):1377–1388.) and with experimental flow data for a binary mixture reported by Cordoba and Schall (Cordoba A. J., Schall C. A. Application of a heat method to determine wax deposition in a hydrocarbon binary mixture. *Fuel* 2001 80:1285–1291). Good agreement in both cases is found.

Key Words: Wax deposition; Modelling; Multicomponent mixture; Non-Newtonian fluids.

INTRODUCTION

Under conditions of constant cooling of pipe walls (i.e., typically in offshore producing platforms), crystal formation and deposition may occur along pipes carrying waxy oil fluids. These solids build up inside the flow-lines and significantly decrease production rates. As crude oils are cooled along the production tubings, a drastic change in the rheological properties of the oil occurs, since hydrocarbon liquids above their cloud point (or wax appearance temperature) behave as Newtonian fluids (Wardhaugh et al., 1988), but below those temperatures they become a shear-thinning and time-dependent suspension (Pedersen and Ronningsen, 2000). The precipitated wax may adhere to cold surfaces and give rise to wax deposition on the walls of the wells.

Some wax will deposit at the inner side of the wall as a consequence of wax precipitation in the bulk oil phase as solid hydrocarbons (Wardhaugh et al., 1988). As the solid fraction increases further to 4–5% near the pour point, the oil turns into a gel with yield stresses, including time-dependent effects and large dependence on the thermal and mechanical history.

Models that incorporate the conservation equations of mass, momentum, and energy have been proposed to predict the wax deposition profile of full-scale pipelines (Burger et al., 1981; Elphingstone et al., 1999; Hsu and Santamaria, 1994; Majeed et al., 1990; Ribeiro et al., 1997; Singh et al., 2000, 2001a, 2001b). A few compositional (i.e., multicomponent) models combining theories of phase-equilibria of multi-component mixtures and fluid mechanics have also been proposed (Goyon et al., 1988; Lindeloff and Krejbjerg, 2002; Ramirez-Jaramillo et al., 2001; Svendsen, 1993).

A number of different assumptions in the calculation of the deposited mass of wax in pipe has been considered in these models, namely molecular diffusion, shear removal, and aging of the wax awing to particle diffusion in the wax gel. Also, different approaches for calculating oil-wax

MARCEL DEKKER, INC.
270 Madison Avenue, New York, New York 10016

equilibria and rheological properties of the fluids have been assumed in these models.

The results on the application of these models are highly dependent on the assumptions and calculation approaches so considered.

In this work, we describe a compositional flow model for wax deposition in pipelines which incorporates phase equilibria, a rheological equation of state and a description of wax adherence to the pipeline walls as a result of the contribution of molecular diffusion, shear removal, and diffusion in the wax gel. As compared to previous models, the present approach incorporates a multicomponent, full non-Newtonian fluid behavior which depends on solid concentration and shear rate, a thermodynamic approach based on a multisolid-phase concept of wax precipitation and a dependence of the radial mass flux of the mixture on the mass density of each liquid fraction, resulted from the equilibrium state at each point of the numerical grid.

In first section, a description of the model is given together with the calculation scheme. In second section, we show the results of the model in three parts: in part (I) the model is first applied to a model mixture. In part (II) a comparison with predictions from a previous model (Svendsen, 1993) is made. Part (III) deals with comparisons between model predictions and experimental flow data. Finally, in third section, a discussion of the model results is given and some concluding remarks are outlined.

MODEL DESCRIPTION

Figure 1a depicts the computational domain, consisting in a model pipe of length L and radius r along which a mixture of hydrocarbons flows. The pipe is divided to form a computational mesh, with boundary conditions applied at the ends and along the exterior surface of the pipe. Finite differences are used in the solution of the differential equations. The model fluid consists of n hydrocarbon components in thermodynamic equilibrium, and therefore their mole fractions in both the liquid and solid phases are functions of pressure and temperature. Since temperature at the external wall of the pipe (which may be assumed to be a vertical oil well) changes axially along the pipe, the forced convection heat transfer process induces a change in the liquid temperature. Convection is included in the heat equation and, in the range of flow rates explored, the diffusion approach from mass transfer is reasonable.

Since both viscosity and wax thickness may change along the pipeline, it is assumed that the wax/oil boundary changes very slowly in the axial direction, so that a quasi steady-state model is applicable for

MARCEL DEKKER, INC.
270 Madison Avenue, New York, New York 10016

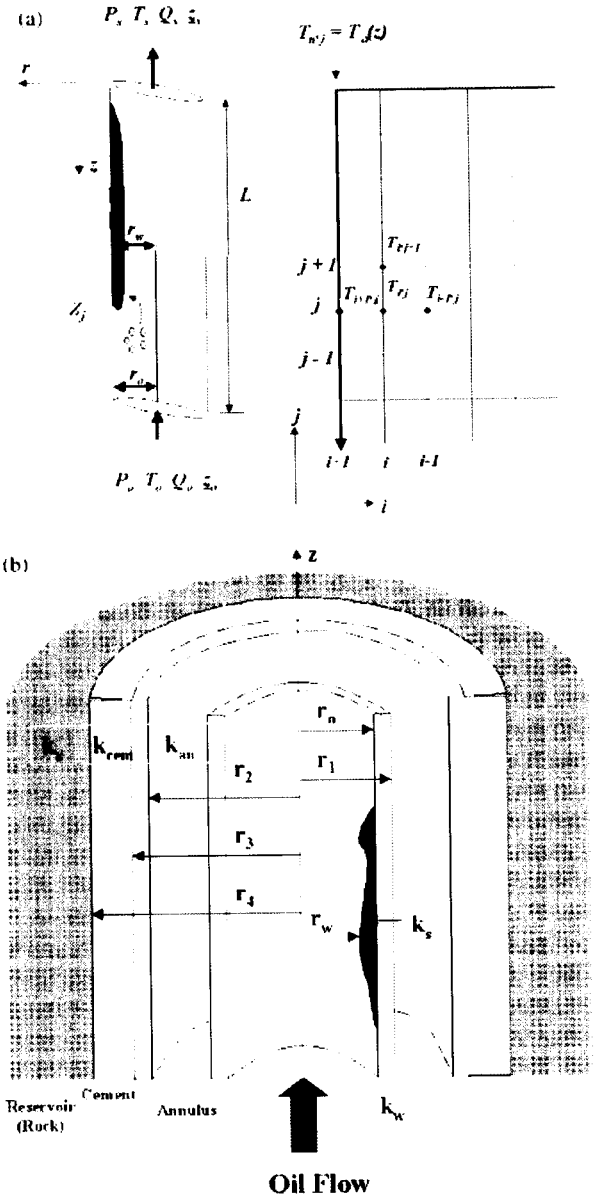

Figure 1. (a) Computational domain for a model pipe. (b) Sections of a model pipe with concentric layers.

MARCEL DEKKER, INC.
270 Madison Avenue, New York, New York 10016

all rate processes concerning energy and mass. Heat associated with frictional heating, axial thermal diffusion and phase transitions are supposed to be negligible compared to heat convection.

The wax deposition rate thus depends on oil composition, oil temperature, external temperature around the pipe, flow conditions, pipeline size and pressure. Wax deposition occurs when the temperature of the deposition surface in the pipe (not the average oil temperature) is below the oil's cloud point temperature. Therefore, the analysis of deposition must mainly include the region close to the inner surface of the pipe, where the process of component radial diffusion, heat flux at the surface, and flow in the boundary layer are linked. The model proposed here incorporates the heat transfer process with constant heat flux at the external wall of the pipe. The reason lies on the fact that the external (geothermal) temperature is know and not the inner wall temperature. The radial temperature gradient and the existing pressure, which drives the flow, induce a radial concentration gradient, assuming that thermodynamic equilibrium of the multicomponent system holds at every stage. The model assumes that the molecules that diffuse to the wall deposit and form a wax layer, which may be removed by shear forces from the fluid. The removal of deposited mass from the layer is especially significant at high Reynolds numbers. In addition, the model includes the diffusion of wax into and within the gel-like deposit, implying that the deposit composition is variable and affects its thickness. The mass flux is calculated for all components in the system and the total flux is the sum of the fluxes of each component.

Model Formulation

The mole fraction of component i in the bulk of the flowing mixture is given by (Svendsen, 1993):

$$z_i = L_x x_i + L_s s_i \qquad (i = 1, 2, \ldots, n) \tag{1}$$

where L_x and L_s are the mole fractions of the liquid and solid phases, respectively, such as:

$$L_x + L_s = 1 \tag{2}$$

and x_i and s_i are the mole fractions of the component i in the liquid and solid phases respectively, such that:

$$\sum_{i=1}^{n} x_i = \sum_{i=1}^{n} s_i = 1 \tag{3}$$

In terms of the weight fractions, Eq. (1) becomes:

$$z_i \mathrm{MW}_i = L_x x_i \mathrm{MW}_i + L_s s_i \mathrm{MW}_i \tag{4}$$

The weight fraction of component i in the feed is:

$$w_i = \frac{z_i \mathrm{MW}_i}{\sum_{p=1}^{n} z_p \mathrm{MW}_p} \tag{5}$$

where the denominator in Eq. (5) is the total molar mass of the liquid feed. The weight fraction of component i in the solid phase in the mixture is w_{si}, where:

$$w_{si} = \frac{L_s s_i \mathrm{MW}_i}{\sum_{p=1}^{n} z_p \mathrm{MW}_p} = \frac{w_i (L_s s_i \mathrm{MW}_i)}{z_i \mathrm{MW}_i} \tag{6}$$

The total weight fraction of wax in the mixture w_s is:

$$w_s = \sum_{i=1}^{n} w_{\mathrm{si}} \tag{7}$$

and the total weight fraction of liquid in the mixture is:

$$w_x = \sum_{i=1}^{n} w_{xi} = \sum_{i=1}^{n} (w_i - w_{si}) = 1 - w_s \tag{8}$$

If V is the volume occupied by 1 mol of solid/fluid mixture, w_s can be expressed as:

$$w_s = \frac{(\sum_{i=1}^{n} L_s s_i \mathrm{MW}_i)/V}{(\sum_{i=1}^{n} z_i \mathrm{MW}_i)/V} = \frac{\rho_s}{\rho_m} \tag{9}$$

where ρ_s and ρ_m are the mass densities of the solid phase and mixture, respectively. The mass density of the liquid phase is:

$$\rho_x = \rho_m - \rho_s \tag{10}$$

Using the mass density of the mixture (Eqs. (9) and (10)) and from the mass balances, the conservation equations for the mixture are given by:

$$\text{Mass} \quad \frac{\partial \rho_m}{\partial t} + \nabla \cdot \rho_m \underline{v} = 0 \tag{11}$$

$$\text{Momentum} \quad \rho_m \left(\frac{\partial \underline{v}}{\partial t} + \underline{v} \cdot \nabla \underline{v} \right) = -\nabla P + \nabla \cdot \underline{\tau} + \rho_m \underline{g} \tag{12}$$

$$\text{Energy} \quad \rho_m C_v \left(\frac{\partial T}{\partial t} + \underline{v} \cdot \nabla T \right) = k \nabla^2 T \tag{13}$$

where $\underline{v}$ is the average macroscopic velocity of the mixture, defined as:

$$\underline{v} = \frac{\sum_{i=1}^{n} \rho_i \underline{v_i}}{\rho_m} \tag{14}$$

and P, $\underline{\underline{\tau}}$ and $\underline{g}$ are the pressure, stress tensor, and gravitational constant, and C_v, k, and T stand for the heat capacity, thermal conductivity (which is assumed constant), and temperature, respectively. It is necessary to point out that the previous conservation equations may also be written in terms of the molar densities or mole fractions of the different components in the two phases.

We also assume quasi-steady state for all rate processes concerning mass, momentum, and energy, and also mixture incompressibility, i.e.,

$$\nabla \cdot \rho_m \underline{v} = 0 \tag{15}$$

The constitutive equation for the fluid is the following modified Casson model:

$$\underline{\underline{\tau}} = 2\eta(\mathrm{II}_D, w_s)\underline{\underline{D}} \tag{16}$$

where the viscosity $\eta(\mathrm{II}_D, w_s)$ is a function of the second invariant of the rate of deformation tensor (II_D) and the solid fraction w_s, and is given by Pedersen and Ronningsen (2000) as:

$$\eta(\dot{\gamma}, w_s) = \eta_{\mathrm{liq}} \exp(A w_s) + B\frac{w_s}{\sqrt{\dot{\gamma}}} + C\frac{w_s^4}{\dot{\gamma}} \tag{17}$$

where η_{liq} is the viscosity of the liquid phase, and A, B, and C are constants. According to Eq. (17), the shear rate-independent term predicts the asymptotic region at high shear rates. The remaining terms express that for high shear rates, the dependence of the viscosity with the solid fraction diminishes, and it is higher at moderate shear rates, according to Pedersen and Ronningsen (2000). The dependence of the viscosity of the liquid phase with temperature is given by the Eyring equation:

$$\eta_{\mathrm{liq}} = E \exp(F/T) \tag{18}$$

where E and F are constants (which were obtained by Pedersen and Ronningsen (2000) by a measuring viscosity data from different North Sea oils).

MARCEL DEKKER, INC.
270 Madison Avenue, New York, New York 10016

The constitutive equation for the mass flux follows Fick's law:

$$\underline{J} = \sum_{i=1}^{n} \underline{J_i} = -D_m \nabla \rho_x = -D_m \frac{\partial \rho_x}{\partial r} \tag{19}$$

The decreased solubility of the wax at the wall temperature induces an increased concentration of precipitated solids next to the wall. This concentration gradient creates a flux of precipitated solids towards the core of the pipe and the liquid is transported to the wall. The concentration created in the liquid phase drives the mass transfer. It is worth mentioning that in most models, the diffusion flux in a multicomponent mixture in the radial direction, is written in terms of the temperature gradient using the chain rule (Svendsen, 1993), although the concentration gradient in Fick's law is subjected to constant temperature and pressure. As it will be shown later, in this work, Eq. (19) is applied to liquid fractions resulting from the thermodynamic equilibrium at a given temperature and pressure, and therefore, is consistent with Fick's law. The quasi steady-state condition implies that the time to establish the heat and mass transfer profiles is short compared with the time for a significant change in the bulk oil temperature at the specific pipe location.

In Eq. (19), D_m is the average diffusion coefficient, which may be expressed as Burger et al. (1981), as:

$$D_m = \frac{C_1}{\eta} \tag{20}$$

where C_1 is a constant to be determined for each oil. Burger et al. (1981), suggested the following expression for this constant:

$$C_1 = 7.4 \times 10^{-8} \frac{T(\psi \mathrm{MW})^{1/2}}{V^{0.6}} \tag{21}$$

(ψ, MW, V are the association parameter, molecular weight, and molar volumes, respectively) and found that $V^{0.6}$ is proportional to T.

It is important to observe that the molecular diffusion transport mechanism states that the concentration gradient of dissolved wax created by the temperature profile induces a flux of this dissolved material toward the wall, where it precipitates and adheres (see: Burger et al., 1981; Ribeiro et al., 1997). This approach to the problem excludes the fact that the dissolved wax in regions away from the wall can sometimes precipitates out of the solution, when the two-phase boundary is surpassed in the bulk. Since at a given stage the solid wax concentration grows in the direction towards the center of the pipe, the transport of solids can be present simultaneously to that of dissolved solids. In fact,

Burger et al. mentioned that "in the situation where there is an increased concentration of precipitated solids near the wall, shear dispersion, and Brownian diffusion would lead to lateral transport and could provide for the movement of solid particles to the wall if a mechanism (i.e., shear removal) was available to remove the solid particles from the solid–liquid interface." This is explicitly shown in their Fig. 9 in Burger et al. (1981), where the initial high concentration of precipitated solids next to the wall diminishes continuously due to transport of solids to the core of the pipe. Subsequently, a stage where the solids concentration is smaller than that in the core is attained, resulting in a net transport of precipitated solids towards the wall. In the simple case of molecular diffusion the diffusive flux occurs in the liquid phase, but if the shear removal mechanism is present, obviously it cannot be assured that the flux of precipitated solids is absent.

On the other hand, the constitutive equation and the momentum balance for the fluid in the pipe may be expressed as:

$$\dot{\gamma}\,\eta(\dot{\gamma},w_s) = \frac{\Delta P}{2L} r \tag{22}$$

where r is the radial distance and $\Delta P/L$ is the pressure gradient that drives the fluid. The variation of the shear rate and viscosity along the radial coordinate are calculated using Eqs. (17) and (22). The radial velocity profile is then readily obtained upon integration from:

$$\dot{\gamma}(r) = \frac{\partial v_z(r)}{\partial r} \tag{23}$$

Integration of the velocity profile leads to the volumetric flow rate:

$$Q = 2\pi \int_0^{r_o} v_z(r) r\, dr \tag{24}$$

If axial thermal diffusion is neglected, the energy balance equation is:

$$v_z(r)\frac{\partial T}{\partial z} = \alpha\left(\frac{\partial^2 T}{\partial r^2} + \frac{1}{r}\frac{\partial T}{\partial r} + \frac{q_h}{k}\right) \tag{25}$$

where α is the thermal diffusivity of the fluid with thermal conductivity k and specific heat capacity. q_h is a heat source term associated with phase transition from the liquid to the solid state, however, an order of magnitude analysis suggests that this contribution is negligible as compared to the other terms in Eq. (25). In addition, the thermal Peclet number P_{eT} (vr/α) is very large, which is the limit found in a real

MARCEL DEKKER, INC.
270 Madison Avenue, New York, New York 10016

situation (Ribeiro et al., 1997). The boundary conditions for Eq. (25) are:

$$T(r,0) = T_o \qquad 0 \le r \le r_o \tag{26a}$$

$$T(0,z) = \text{finite} \qquad z > 0 \tag{26b}$$

$$-k\frac{\partial T}{\partial r}\bigg|_{r=r_w} = U[T(r_w,z) - T_\alpha(z)] \tag{26c}$$

Equation (26c) is the boundary condition corresponding to the cooling of the liquid due to the temperature gradient existing between the geothermal temperature of the rock in contact with the exterior pipe wall $T_\alpha(z)$ and the temperature of the liquid in contact with the deposited layer $T(r_w,z)$ (See Fig. 1a). The global heat transfer coefficient U is given as the sum of the resistances (in terms of the respective radii and thermal conductivity k) of the solid phases corresponding to the cement layer, annulus, pipe wall, wax, and the resistance due to the interface solid–liquid h_{in}^{-1}:

$$U = \frac{1}{r_w}\left(\frac{1}{k_{\text{cem}}}\ln\frac{r_4}{r_3} + \frac{1}{k_{\text{an}}}\ln\frac{r_2}{r_1} + \frac{1}{k_w}\ln\frac{r_1}{r_0} + \frac{1}{k_s}\ln\frac{r_0}{r_s} + \frac{1}{h_{\text{in}}r_w}\right)^{-1} \tag{27}$$

where the deposited gel thermal conductivity is assumed to be a function of its wax content (F_w) given by (Singh et al., 2000):

$$k_s = \frac{[2k_{\text{wax}} + k_{\text{oil}} + (k_{\text{wax}} - k_{\text{oil}})F_w]}{[2k_{\text{wax}} + k_{\text{oil}} - 2(k_{\text{wax}} - k_{\text{oil}})F_w]}k_{\text{oil}} \tag{28}$$

and the interfacial heat transfer coefficient in laminar flow is given by:

$$h_{\text{in}} = 1.86\left(\frac{k_b}{d}\right)\left(\text{Pe}\frac{d}{L}\right)^{1/3}\left(\frac{\eta_b}{\eta_o}\right)^{0.14} \tag{29}$$

It should be remembered that the heat transfer process has been modeled by the convection–diffusion equation (25), which has a convection term in the axial direction and a diffusion term in the radial direction. Hence, diffusion of heat and mass exists in the radial direction whereas heat is transferred by convection along the axial direction.

In Fig. 1b, a section of the pipe with the mentioned concentric layers is depicted. Equation (27) takes into account the variation of deposited layer thickness and therefore the global heat-transfer coefficient changes with axial distance and with the deposited solid fraction (Lindeloff and Krejbjerg, 2002).

MARCEL DEKKER, INC.
270 Madison Avenue, New York, New York 10016

To account for pressure and temperature effects on wax-formation equilibria, a multisolid-wax equilibrium formulation (Lira-Galeana et al., 1996) that uses an equation-of-state (EOS) is employed in this work. This approach is based on the experimentally-supported (Pedersen et al., 1991; Snyder et al., 1991) assumption that, upon crystallization, the precipitated species from petroleum do not form a solid solution but instead, a multisolid-wax precipitation process which considers only a limited number of solid hydrocarbons is undergone. This method differs from other algorithms (Coutinho and Ruffier-Meeray, 1997; Erickson et al., 1993; Hansen et al., 1988; Lindeloff et al., 1999; Pauly et al., 2000; Won, 1986) in which a solid solution concept for the precipitated wax is assumed.

In terms of component fugacities, Lira-Galeana et al. showed that the following phase-stability test based on the use of the EOS suffices for determining the number and identity of the precipitated solids, i.e.,

$$f_i(P, T, \underline{z}) - f^{s}_{\text{pure},i}(P,T) \geq 0 \qquad i = 1, 2, \ldots, N \tag{30}$$

At any given pressure and temperature condition, the mixture species that fulfill the above expression will precipitate, and those which do not, will only be present in the liquid (i.e., oil) phase. Further material-balance equations together with a multivariable Newton–Raphson or more sophisticated solution procedures can be used to complete the computational algorithm. Details are given in Pan et al. (1997) and in Lira-Galeana and Hammami (2000). Further application of this method can be seen in the works of Nichita et al., (1999, 2002), Pan and Firoozabadi (1998).

Since the thermodynamic equilibrium requires that the fugacity of each component in the liquid phase be equal to the fugacity of the pure components in the solid phase, it is required to perform an equilibrium calculation at a given temperature and pressure at each point of the grid domain. This will give the precipitated solid fractions and liquid gradients from which the mass flux calculations for each component of the mixture (Eq. (19)) can be carried out.

The total amount of deposited mass at time t and distance from inlet $z = 0$ to $z = L$ (i.e., from bottom to the surface) can be expressed as the sum of three contributions:

$$M(t, z) = \sum_{i=1}^{n} M_{\text{MD}i}(t, L) - M_{\text{SR}}(t, L) - M_{\text{GD}}(t, L) \tag{31}$$

where $M_{\text{MD}i}(t, L)$ is the deposited mass due to molecular diffusion for each component in the mixture, $M_{\text{SR}}(t, L)$ is removed mass due to the

shear removal mechanism and $M_{GD}(t, L)$ is the mass of wax molecules diffusing into the gel deposit.

The shear removal mechanism assumes that hydrodynamic forces remove a portion of the deposited layer. In this work, we use an approach for estimating the removal rate from the work published by Solaimany Nazar et al. (2001), who used Kern and Seaton (1959) expression for estimating the removal rate which is suggested to be proportional to the deposited mass and the wall shear stress exerted by the flowing fluid. This can be expressed as:

$$J_{SR} = A_1 \exp(-B_1/T)\tau_w M(t - dt, z) \tag{32}$$

where A_1 and B_1 are constants that depend on the oil composition and for each crude oil must be determined experimentally, T is the current temperature of the fluid, $M(t-dt, z)$ is the deposited mass one step before the current time, and the wall shear stress is given by:

$$\tau_w = \frac{\Delta P}{L}\frac{r_w}{2} \tag{33}$$

The formation of solid wax crystals deposited on the walls leads to the formation of a gel layer (Kané et al., 2003; Singh et al., 2000, 2001a, 2001b), which consists of a liquid phase and a nonmoving solid phase. The gel layer behaves as a porous medium, in which wax molecules continue to diffuse due to the radial variation of temperature. The aging of the gel is manifested by an increase of the wax content of the deposited gel. Therefore, in addition to the processes of molecular diffusion and shear removal, there is also an internal diffusion process. A temperature gradient across the gel layer exists and hence, there is an internal diffusion flux of wax within the gel deposit. Singh et al. (2000) suggest the following expression for the internal diffusion:

$$J_{GD} = -D_e \frac{dC_{ws}}{dT}\frac{dT}{dr} \tag{34}$$

where the derivative of the solubility with respect to temperature (dC_{ws}/dT) is given directly from the thermodynamic multisolid equilibrium model (Lira-Galeana et al., 1996). The effective diffusivity of wax molecules into the gel deposit is a function of the porosity of the gel. The following expression derived for porous media of flake-like particles (Cussler et al., 1988) is used for the effective diffusivity:

$$D_e = \frac{D_{wo}}{1 + \alpha^2 F_w^2/(1 - F_w)} \tag{35}$$

where the molecular diffusivity D_{wo} of paraffins in paraffinic solvents has been proposed by Hayduk and Minhas (1982) to be $1.48 \times 10^{-6}\,cm^2/s$. α is the average aspect ratio of wax crystals and the weight fraction of solid wax in the gel is given by:

$$F_w = \frac{\text{mass of wax}}{\text{mass of wax} + \text{mass of oil}} = \frac{M(t, L)}{\rho_{gel}\pi(r_0 - r_w)^2 \Delta z} \tag{36}$$

the density of the gel (ρ_{gel}) is constant and does not vary with time. Equation (31) becomes:

$$M(t, L) = \sum_{i=1}^{n} M_i(t, L) = \sum_{i=1}^{n} 2\pi \int_0^t \int_0^L r_w J_{MDi}|_{r=r_w}\, dz\, dt - 2\pi \int_0^t \int_0^L r_w J_{SR} dz\, dt + 2\pi \int_0^t \int_0^L r_w J_{GD}\, dz\, dt \tag{37}$$

where the mass flux (Eq. (19)) is evaluated at the liquid–solid interface ($r = r_w$). The removal rate is calculated taking into account the mass previously deposited (i.e., at time $t-dt$). The derivative of M is:

$$\frac{\partial M}{\partial z} = \pi(r_o^2 - r_w^2)\rho_w = \sum_{i=1}^{n} \frac{\partial M_i}{\partial z} = \sum_{i=1}^{n} 2\pi \int_0^t r_w J_{MDi}|_{r=r_w}\, dt - 2\pi \int_0^t r_w J_{SR}\, dt + 2\pi \int_0^t r_w J_{GD}\, dt \tag{38}$$

Equation (38) is an implicit equation for r_w. Having found r_w, the total deposition rate is:

$$\frac{dM}{dt} = \sum_{i=1}^{n} \frac{dM_i}{dt} = \sum_{i=1}^{n} 2\pi \int_0^L r_w J_{MDi}|_{r=r_w}\, dz - 2\pi \int_0^L r_w J_{SR}\, dz + 2\pi \int_0^L r_w J_{GD}\, dz \tag{39}$$

Appendix I presents a flow diagram for the entire calculation scheme. Input variables for a given calculation as well as output quantities and are all illustrated in Table 1.

Table 1. Input and calculated variables for the flow chart calculation procedure (see Fig. 1a).

Input data	Output data
P_o	$P^*(r, z)$
T_o	$T^*(r, z)$
P_s	Solid fractions (w_s)
T_s	Density (ρ)
$\underline{z}$	Viscosity (η)
r	Radial mass flux (J_i)
L	Mass deposited (M_w)
$T_\alpha(z)$	

RESULTS AND DISCUSSION

1. Model Pipe

Before dealing with comparison with experiments, we first show an example of a model oil, whose composition includes heavy components, to analyze the effect of heavy fractions on deposition. This sample case have typical values of geometry and flow rate that render a range of Reynolds numbers. Input data for the system are given in Table 2. The weight fractions and molecular weights of the mixture components are given in Tables 3 and 4.

Although in some particular simplified cases it is possible to give analytical asymptotic expressions for the mass and heat transfer problems (for example, the Graetz problem with Neumann boundary conditions at high Reynolds numbers), implementation of the thermodynamic equilibrium relations for multicomponent mixtures precludes any effort in that direction. Moreover, the use of numerical methods is further justified due to the nonlinearity of the rheological constitutive equation, which gives rise to a highly nonlinear velocity profile that changes as the solid fraction concentration is modified by the thermodynamic equilibrium.

The calculations are performed from the bottom of a model oil pipe up to the surface. Given a "geothermal" (imposed) axial temperature profile, the heat flow is transferred across the pipe wall, so that the liquid temperature diminishes along the pipe from bottom to surface conditions. The heat transfer mechanism is mostly concentrated in a thin thermal boundary layer, which, under the applied conditions, its width

Table 2. Input information for the model pipe.

Model parameters	Values
r_o (m)	0.0445
r_1 (m)	0.05
r_2 (m)	0.08
r_3 (m)	0.10
r_4 (m)	0.12
T_o (K)	381.28
T_s (K)	303
P_o (bar)	318.82
P_s (bar)	56.44
L (m)	3660
Q (m^3/h)	143
t (h)	3744
Δt (h)	37.44

Table 3. Weight fraction composition for mixture.

Hydrocarbon	Molecular weight (kg/kmol)	Weight fraction
n-C_{15}	212.47	0.7173
n-C_{20}	282.62	0.2400
n-C_{25}	352.77	0.0180
n-C_{30}	422.92	0.0102
n-C_{35}	493.07	0.0089
n-C_{38}	535.16	0.0035
n-C_{40}	563.22	0.0011
n-C_{42}	591.28	0.0007
n-C_{45}	633.37	0.0001

is smaller than the momentum boundary layer. The numerical algorithm requires the discretization of the cylindrical domain into a grid with coordinates (r, z). Starting from known volumetric flow rate Q, T_o, and P_o (temperature and pressure at the bottom of the well) and initial composition of the liquid fractions, the pressure gradient must be calculated. Initially, and predicted by Eq. (30), no solid fractions in the liquid are present, so the liquid is Newtonian with viscosity and mixture density given by the initial conditions of pressure and temperature. The

Table 4. Input information for the system in the previous model.

Parameter	Value
r_o (m)	0.0045
L (m)	1.000
Q (m^3/h)	0.050
MW_1 (kg/kmol)	215
MW_2 (kg/kmol)	530
Re	193
T_o (K)	303
w_1	0.850
w_2	0.150
T (h)	80
Δt (h)	0.03

parabolic velocity profile is considered in the case of laminar Newtonian flow for the calculation of the temperature profile along the following axial grid point using Eq. (25). Knowing the updated values of pressure and temperature at the points $(r_0+\Delta r,\ z_0+\Delta z)$, the thermodynamic equilibrium will give the corresponding solid fractions, depending on the phase boundary envelope. The calculation of the solid fractions in equilibrium assumes that equilibrium conditions are reached immediately at each grid point, so the quasi-steady-state approximation holds. As soon as liquid fractions are known, they diffuse according to Eq. (19), with diffusion coefficient given by Eqs. (20) and (21). From the resulting fractions and the calculated temperature gradient, the mass flux may be evaluated at the wall for each species. Equation (39) provides the deposition rate, which is a function of the mass flux and r_w, the removal rate and the diffusion of waxes into the gel.

With the presence of large amounts of solid fractions, the fluid gradually becomes non-Newtonian and shear-rate dependent. The shear rate radial profile is calculated from Eqs. (17) and (22) given the equilibrium solid concentrations and a guessed value of the pressure drop. Equations (23) and (24) provide the velocity profile and the volumetric flow rate. We must satisfy a local mass balance expressed as follows:

$$\begin{pmatrix}\text{Mass flow of oil}\\ \text{fed from cell } i\\ \text{to cell } i+1\end{pmatrix} = \begin{pmatrix}\text{Mass flow of oil}\\ \text{leaving cell } i\end{pmatrix} - \text{Deposited mass}$$

$$(\rho_m)_{i+1}Q_{i+1} = (\rho_m)_i Q_i - \left.\frac{dM}{dt}\right|_{i+1} \tag{40}$$

MARCEL DEKKER, INC.
270 Madison Avenue, New York, New York 10016

where $(dM/dt)|_{i+1}$ is the deposition rate from cell i to cell $i+1$, and which is given by:

$$\left.\frac{dM}{dt}\right|_{i+1} = \sum_{k=1}^{n} \frac{dM_k}{dt} = \sum_{k=1}^{n} 2\pi \int_z^{z+\Delta z} r_w J_{\mathrm{MD}i}|_{r=r_w}\, dz - 2\pi \int_z^{z+\Delta z} r_w J_{\mathrm{SR}}\, dz + 2\pi \int_z^{z+\Delta z} r_w J_{\mathrm{GD}}\, dz \tag{41}$$

The pressure is updated to calculate the next temperature profile. The iterative process is repeated until the conditions at the surface of the wall (i.e., when $z = L$) are satisfied (i.e., P_s and T_s, namely the pressure and temperature at the pipe surface). The numerical method used to solve the equations has been described elsewhere (Ramirez-Jaramillo et al., 2001). The following results are given for oil model.

In Fig. 2, the geothermal axial temperature profile of the rock in contact with the exterior wall (which occur in the case of a vertical oil well) of the pipe is shown. The geothermal temperature decreases from 380 to 300K almost linearly, but over the remaining 1000 m from the inlet, the temperature decreases more steeply to 300K.

Figure 3 depicts the calculated pressure profile along the well. Pressure decreases almost linearly from around 325 bar at the bottom of the well

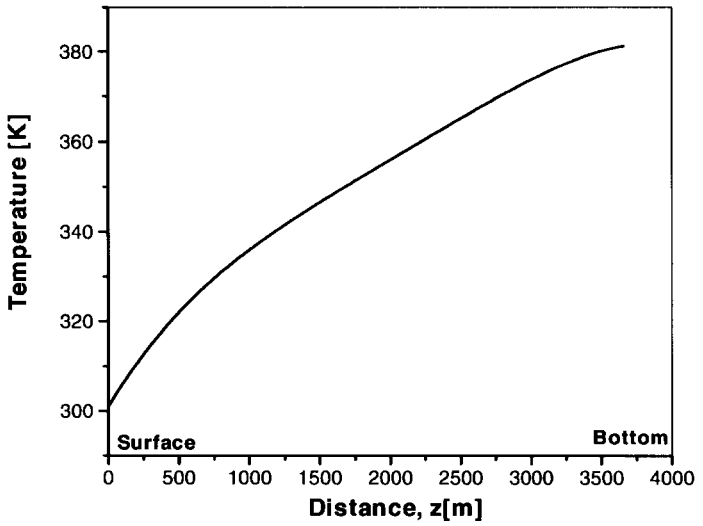

Figure 2. Geothermal axial temperature profile of the model oil well.

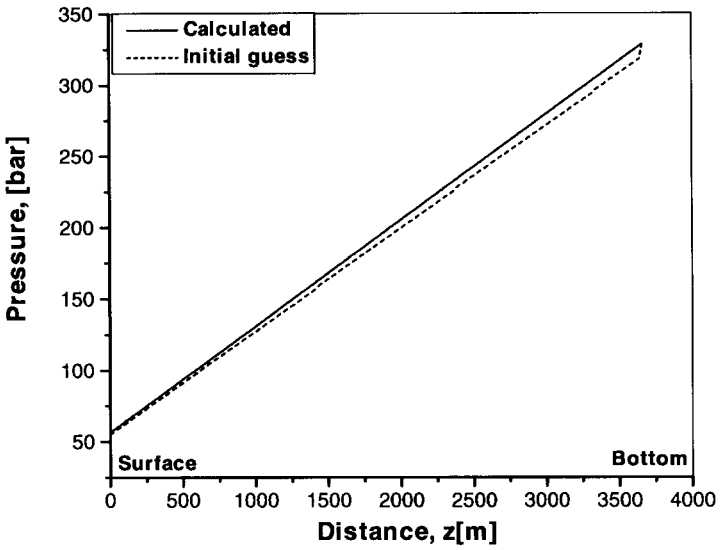

Figure 3. Guess and calculated pressure profile for the mixture.

to approximately 50 bar at ground conditions. These pressure values are considered in the calculation of the thermodynamic equilibrium at each axial grid point. Since the pressure gradient is almost constant, the flow rate is expected to be a decreasing function of the axial coordinate due to wax deposition.

The 80K decrease in temperature along the well length and the appearance of solid fractions results in a substantial increase in the viscosity of the mixture. In Fig. 4, the viscosity of the mixture shows a three-fold increase along the well length. In the same figure, the volumetric flow rate is plotted with axial distance. Under laminar conditions, the flow rate is inversely proportional to the mixture viscosity and depends strongly on the pipe effective radius. A substantial decrease in the volumetric flow rate as the fluid reaches the inlet is thus predicted. This decrease in the volume of fluid per unit time is compensated by an increment in the mixture density (see Fig. 5), to keep the balance of the mass rate per unit time along the pipe. The viscosity of the liquid decreases with the shear rate, it increases with the solid fractions and decreases with temperature. The behavior exposed in Fig. 4 is thus the resulting viscosity given by Eqs. (17) and (22), where all these variables are taken into account.

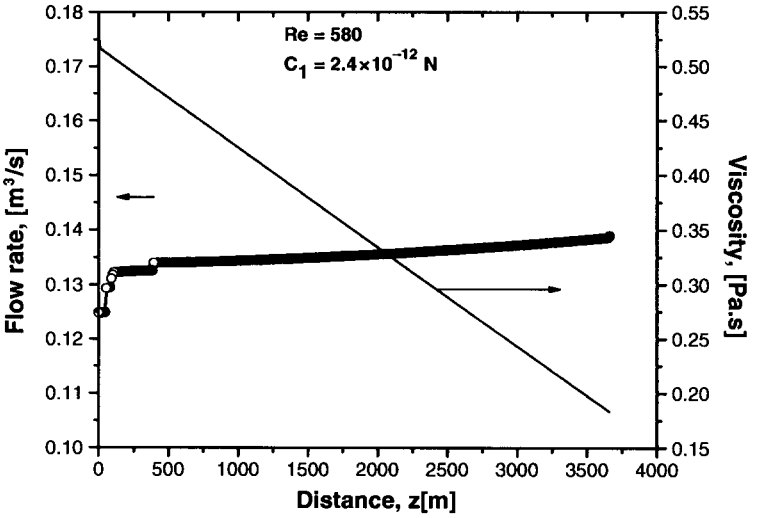

Figure 4. Mixture shear viscosity and volumetric flow rate plotted with axial distance referred to the inlet coordinate for mixture.

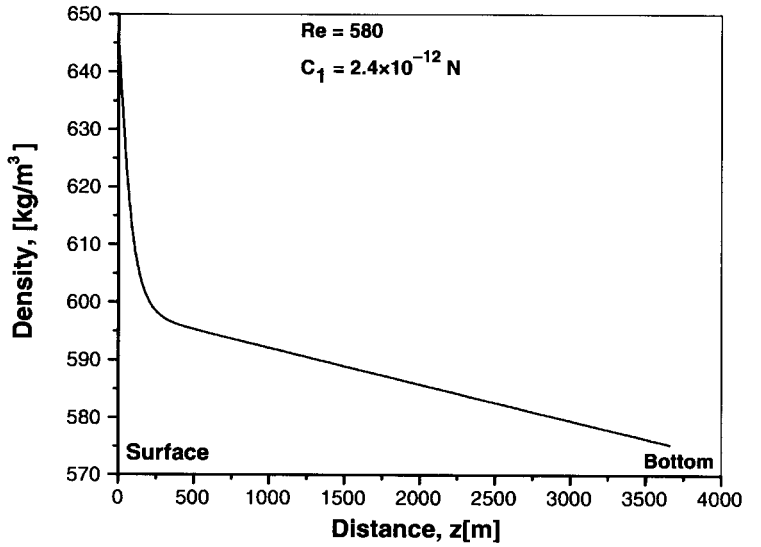

Figure 5. Variation of the density profile with axial distance for model oil.

The fluid viscosity also varies along the radial coordinate. The shear rate is zero at the pipe center and increases up to the wall region, where the velocity of the liquid decreases to zero. The viscosity thus should decrease as the wall is approached, but this effect is overcome by the increase in the viscosity due to the low temperature of the region in contact to the wall and to the presence of solid fractions in this region. In the whole, the radial viscosity profile changes axially in a pronounced nonlinear form along the pipe axis.

Results show that the value of the diffusion constant in Eqs. (20) and (21) influences strongly the amount of solid fractions deposited on the wall and hence the width of the deposited layer. Equation (21) states that C_1 is a function of the average molecular weight of the mixture and the association parameter. To quantify the effect of the variation of C_1 on the resulting deposition rate, we choose two extreme values, i.e., 2.4×10^{-12} and 1×10^{-10}. This will provide two values of the average diffusion constant and hence a variation in the mass Peclet number. In Fig. 6, we show the total solids deposition as a function of the Reynolds number for 156 days of flow time, considering the two values of C_1. There is a strong

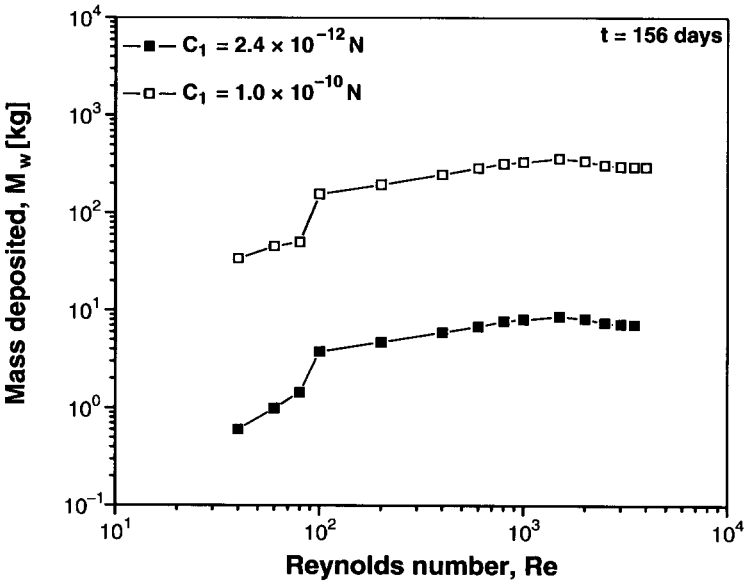

Figure 6. Overall solids deposition mass (kg) vs. Reynolds number after 156 days of flow time, for two values of C_1. Inset is a log–log plot.

effect of the flow and magnitude of the diffusion constant on the total deposition, specifically in the low range of Reynolds numbers. The solids deposition increases steeply with Reynolds number up to Re $\approx$ 100, where a more gradual increase is observed for higher Reynolds numbers. It is very interesting that at very high Reynolds numbers (more than 2000) the mass deposited decreases with Re after describing a maximum. This result is ascribed to the influence of the shear removal process when the shear stress attains large magnitude, which is consistent with similar predictions found in the current literature.

The proposed model can determine the point along the well length where solids start depositing. As the liquid mixture flows along the pipe from bottom to the surface of the well, the liquid is cooled and may surpass the liquid–solid equilibrium envelope. As depicted in Fig. 7, the solid weight fraction suspended in the liquid reaches the solid–liquid equilibrium phase boundary close to 391 m depth. Thereafter, closer to the inlet, the weight fraction increases steeply up to the exit, reaching values around 2.7 wt% close to the ground. In Fig. 8, it is shown that the layer thickness reaches a maximum at around 270 m depth, and the width of the layer increases with Reynolds number. A maximum in the layer thickness has been also predicted in the current literature

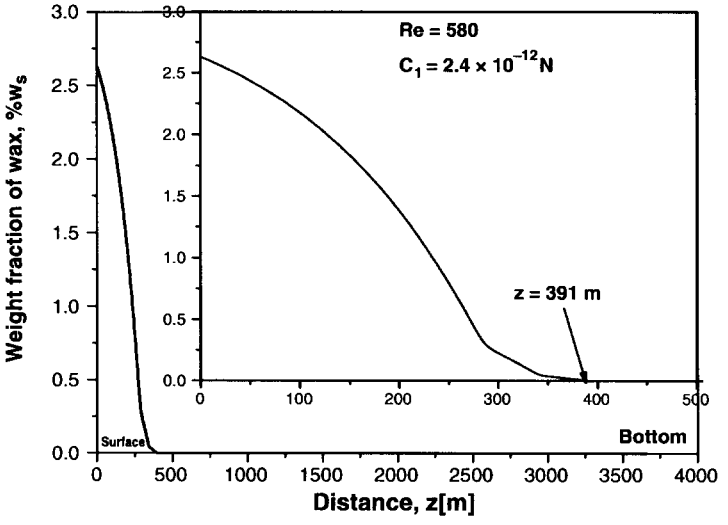

Figure 7. Variation of the solids fraction as a function of the axial coordinate after 156 days of flow time.

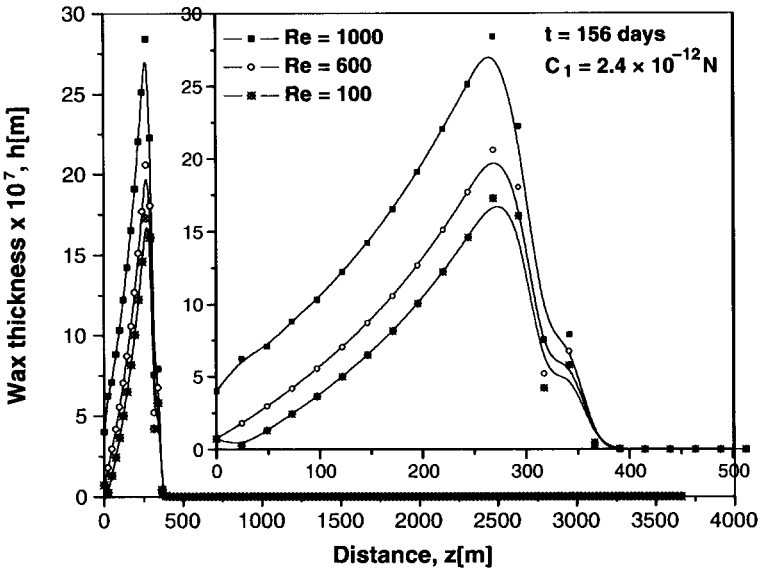

Figure 8. Deposited layer thickness as a function of the axial coordinate for the mixture, for various Reynolds numbers with $C_1 = 2.4 \times 10^{-12}$ N.

(Majeed et al., 1990). The initial increase in the thickness is due to the increase in solids fraction, but as the liquids experiences further cooling the temperature gradient between the fluid and the wall diminishes as the exit is approached. Since the radial temperature gradient is the driving force for radial diffusion, a reduction in the magnitude of the mass flux is then induced, causing a diminishing deposition rate and lower amount of mass deposited.

It is also possible to calculate the change in the thickness of the deposited layer as a function of flow time. As depicted in Fig. 9, the width of this layer increases substantially for flow times larger than 100 days.

In Fig. 10 the contributions from molecular diffusion, diffusion in the gel phase and shear removal on the mass rate are plotted as a function of axial distance, for a given Re number and flow time. At this flow rate, the contribution of diffusion into the gel phase is very substantial, especially close to the surface of the well, as opposed to the shear removal process.

In Fig. 11 shows that, by varying parameter C1 of the model (according to either deposition data or pressure–temperature dynamic

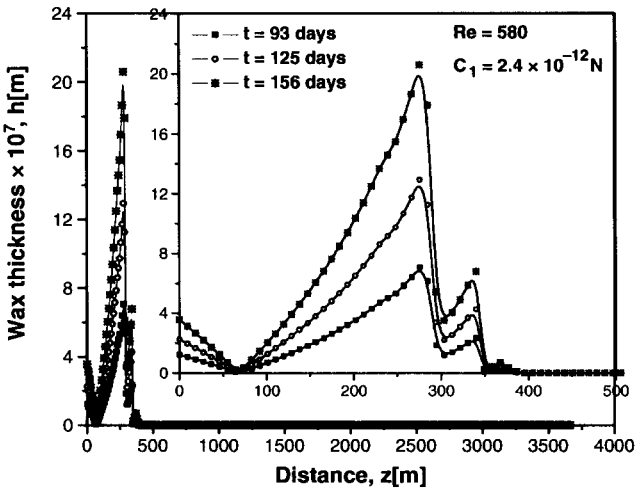

Figure 9. Deposited layer thickness as a function of the axial coordinate for the mixture, for various values of the flow time, and for $C_1 = 2.4 \times 10^{-12}$ N.

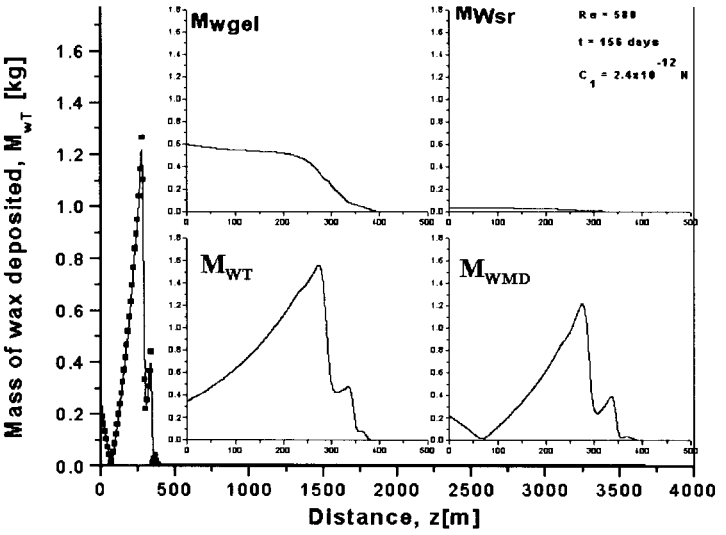

Figure 10. Contributions from molecular diffusion (M_{WMD}), diffusion in the gel phase (M_{Wgel}) and shear removal (M_{WSR}) to the mass deposited (M_{WT}) as a function of axial distance, for a given Re number and flow time.

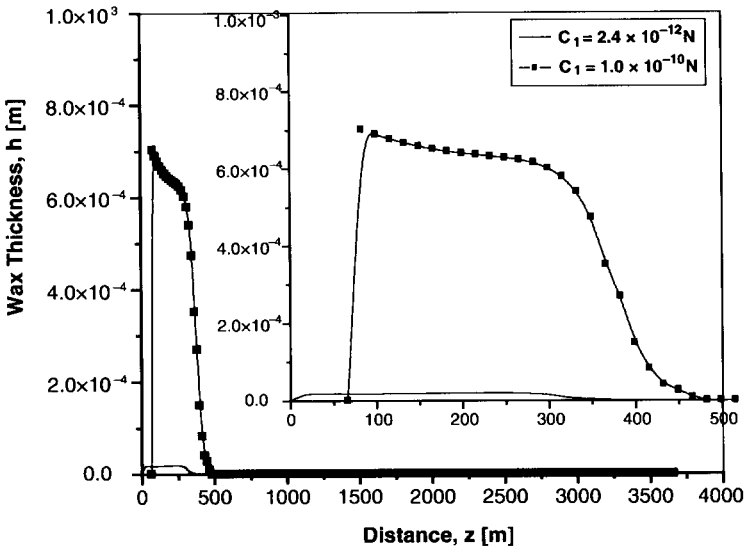

Figure 11. Effect of parameter C_1 on the growth of the wax thickness, h. The wax thickness grows ~100 times.

logs within a well), reasonable wax-thickness values can easily be obtained. In several parts of the manuscript we have pointed out that the growth of the solids layer depends strongly on the mass diffusion coefficient (Eq. (20)). Other researchers have given a range of values to the constant C_1 in Eq. (20) to model their systems. This is of course, not an exact procedure, but an approximated approach. The fact that this coefficient is not provided for the system under consideration led us to choose a given value. However, the layer growth can increase if we allow a higher value of C_1 within the mentioned range, as the Fig. 11 shows for two arbitrary values of such a variable parameter.

2. Comparison With a Previous Model

Results from the present model are compared with numerical results reported by Svendsen (1993), who used a similar flow model, but without the contributions of shear removal nor diffusion in the gel phase. Therefore, in this comparison, we do not consider the mechanisms of

shear removal and gel diffusion. As in the present model, Svendsen assumes essentially that the deposition will only occur if the wall temperature of the pipe is below the precipitation temperature of the oil. Therefore, a negative temperature gradient must be present in the oil. The wall friction must be so large that wax crystals can stick to the wall. Finally, it is further assumed that the wax/oil boundary moves so slowly that a quasi steady-state model is applicable for all rate processes concerning energy and mass. The system consists of a hydrocarbon mixture with two phases, solid and liquid. The solid phase of the mixture is referred to as wax particles. If these particles stick to the wall, wax deposition occurs.

Input data for the present comparison is shown in Table 4. Constant wall temperature may be considered as a boundary condition for the temperature distribution. However, as mentioned above, if the thermal conductivity of the deposit is very different to that of the oil, then the constant heat flux boundary condition is convenient. Equation (26c) is the boundary condition corresponding to the cooling of the liquid due to the temperature gradient existing between the geothermal temperature of the rock in contact with the exterior pipe wall $T_\alpha(z)$ and the temperature of the liquid in contact with the deposited layer $T(r_w, z)$.

The global heat transfer coefficient U is given as the sum of the resistances (in terms of the respective radii and thermal conductivity k) of the solid phases corresponding to the cement layer, annulus, pipe wall, wax, and the resistance due to the interface solid–liquid h_{in}^{-1}, as shown in Eqs. (27) and (28). Two hydrocarbon components are used in the simulations.

In Fig. 12, the predicted temperature profiles of the two models are compared. The model presented in this work predicts a larger temperature gradient and more complex profile next to the wall. Differences indicate that the velocity profiles of each model are different. In fact, in the present model, a full non-Newtonian profile, which depends on the shear rate and solid concentration is considered in the convection–diffusion equation for the temperature, Eq. (25), whereas in Svendsen's model, a power-law profile is taken into account.

In Fig. 13, a comparison is made on the predictions of the ω_i functions defined in terms of the solid fractions of the ith component w_{si} as:

$$\omega = \sum_{i=1}^{n} \omega_i = \sum_{i=1}^{n} \left[-T \frac{\partial w_{\text{si}}}{\partial T} + (w_i - w_{\text{si}}) \frac{T}{\rho_m} \frac{\partial \rho_m}{\partial T} \right] \tag{42}$$

MARCEL DEKKER, INC.
270 Madison Avenue, New York, New York 10016

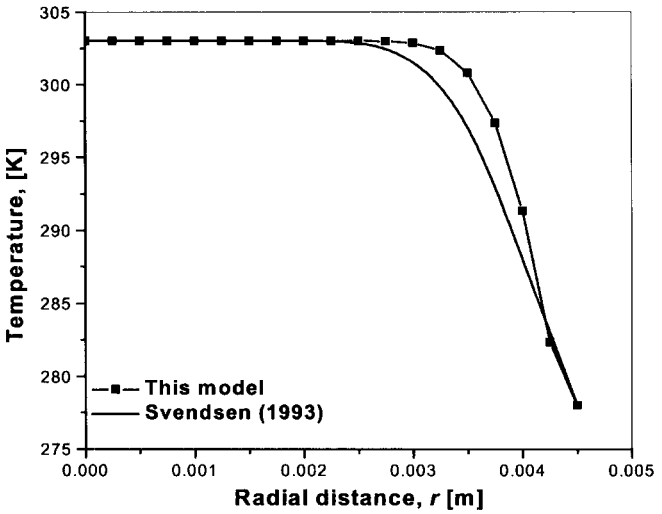

Figure 12. Comparison of predictions from Svendsen model (Svendesen, 1993) and the present model of the radial temperature profile.

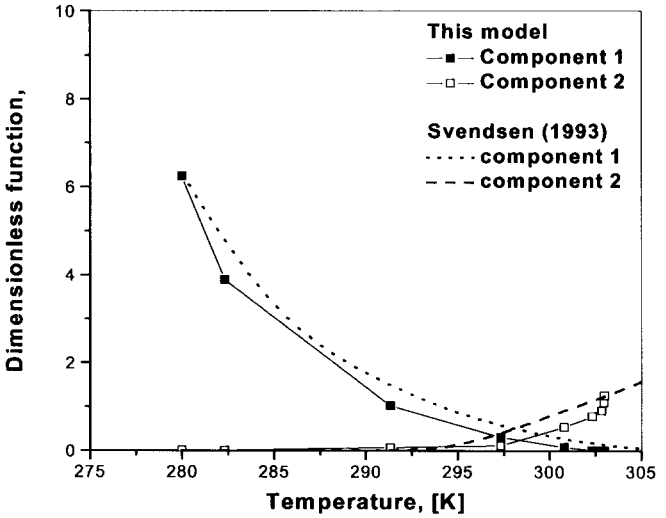

Figure 13. Variation of the ω_i functions with temperature for the two-component mixture. Predictions from the present model and those from Svendsen (1993).

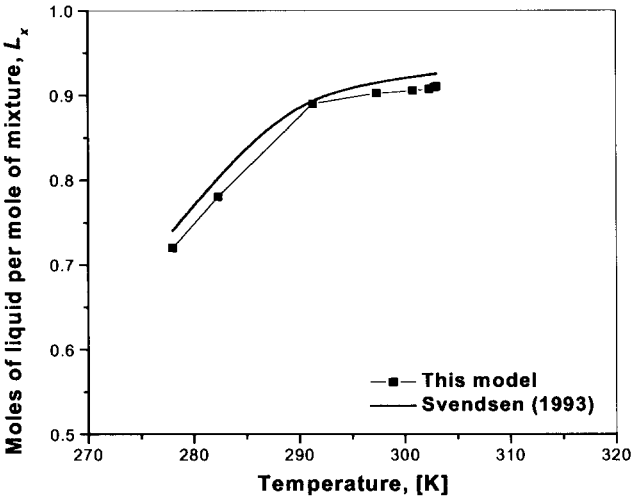

Figure 14. Comparison of number of moles in liquid phase per mole mixture as a function of temperature. Model prediction.

The mass flux $\underline{J}$ is given in terms of the temperature gradient as (Svendsen, 1993):

$$\underline{J} = -D_m \frac{\partial \rho_x}{\partial T} \frac{\partial T}{\partial r} = -D_m \rho_m \omega \frac{1}{T} \frac{\partial T}{\partial r} \tag{43}$$

where D_m is the average diffusion constant. Figure 13 describes the variation of the ω function with temperature for both models. The lightest component (component 1), which has the largest weight fraction, contributes more to the deposition rate in the temperature interval 280–298K, due to the thermodynamic equilibrium.

In Fig. 14 the calculated liquid fraction is plotted with temperature. The predictions of both models are in quantitative agreement, indicating that for pipeline temperatures higher than 305K, the mixture is reaching a full liquid phase state. The wax appearance point (WAP) for this mixture is 319K.

In Figs. 15 and 16 we compare results of the two models in the small-scale close system. It is assumed that the inner wall of the loop is kept at a temperature higher than the wax appearance temperature, except in the test section. The simulation flowing time is 80 h. Deposition as a function of time is shown in Fig. 15 per m^2 of clean wall, and the wax thickness

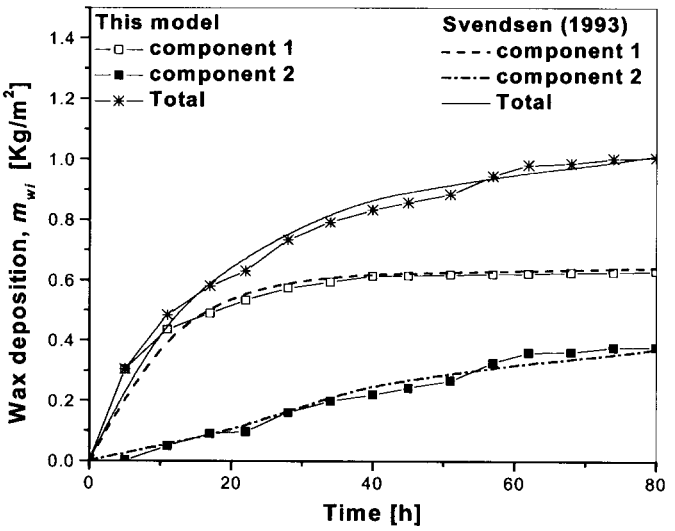

Figure 15. Total deposited mass per unit area as a function of time. Axial distance from inlet = 0.5 m. Model predictions for a two-component mixture.

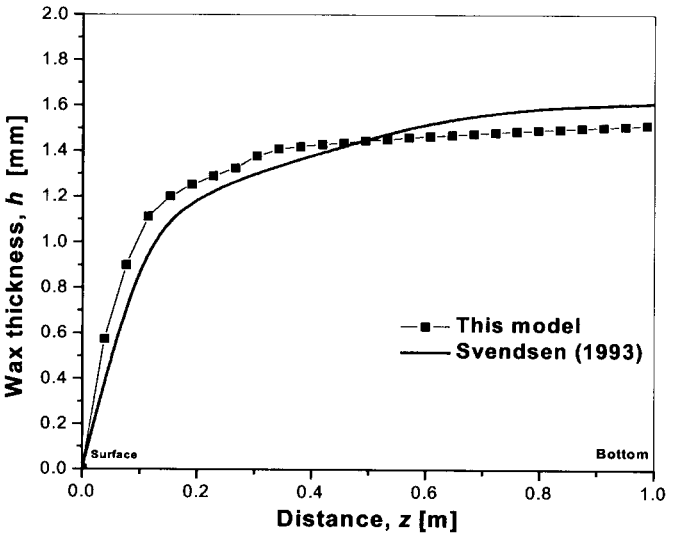

Figure 16. Model predictions of the wax layer-thickness vs. the axial coordinate.

MARCEL DEKKER, INC.
270 Madison Avenue, New York, New York 10016

distribution after a flow time of 80 h is shown in Fig. 16. A very close agreement is depicted between the two models. Figure 15 shows that during the first hours of flow the wax deposition is entirely due to the lightest component. At the wall temperature of the test section (278K) ω_1 is much larger than ω_2, as shown in Fig. 13, and therefore $J_1 \gg J_2$. However, at temperatures larger than 298K, ω_2 dominates over ω_1 and then $J_2 \gg J_1$.

3. Comparison With Experimental Flow Data

Finally, we compare predictions of our full model with the experimental results from Cordoba and Schall (2001) who measured the deposition behavior of a model binary mixture using a flow-loop device. Here, the resistance to heat transfer from the internal flowing fluid to the environment consists of the resistance of the interface liquid-wax, heat conduction through the wax, heat conduction through the pipe wall, pipe wall-environment interface. The geometry of the test section considered is illustrated in Fig. 17.

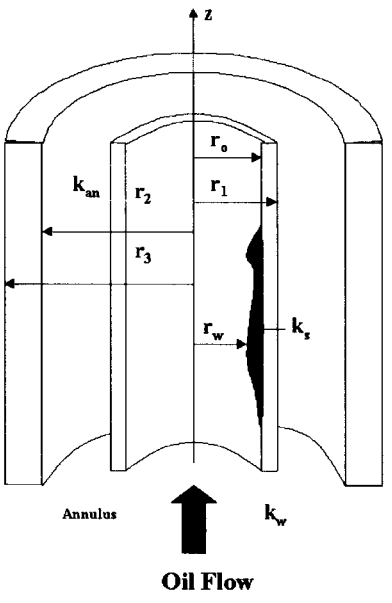

Figure 17. Sections of a flow system used by Cordoba and Schall (2001).

Table 5. Input information for the comparison with experimental flow data.

Parameter	Value
r_o (m)	0.001841
r_1 (m)	0.003175
r_2 (m)	0.003301
k_a (W/m K)	19.5
k_{an} (W/m K)	0.504
k_w (W/m K)	17.3
L (m)	0.254
Q (m^3/s)	1.0×10^{-6}
Re	526
T_p (K)	273.15
MW1 (C_8) (kg/kmol)	114.232
MW2 (*cyclo* C_6C_{19}) (kg/kmol)	350
T (h)	2
Δt (h)	0.133

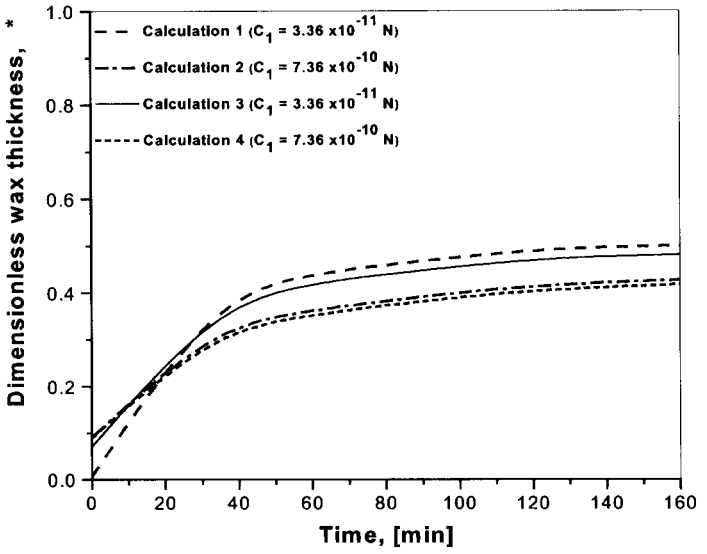

Figure 18. Predictions from the present model of the dimensionless wax thickness distribution with time for different *cyclo* C_6C_{19}:C_8 ratios given in Table 6.

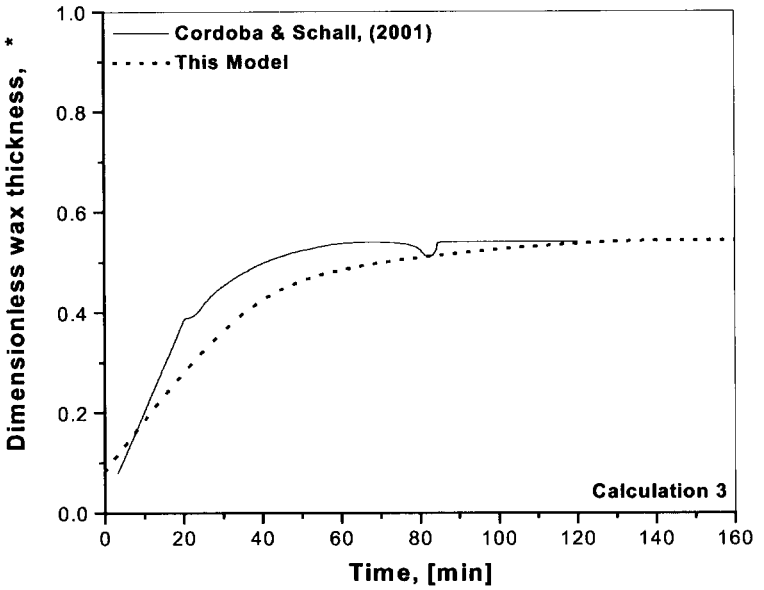

Figure 19. Comparison of model predictions and Cordoba and Schall (2001) data of the dimensionless wax thickness distribution for the 90:10 (*cyclo* C_6C_{19}:C_8) ratio.

The system under analysis consider two hydrocarbon components *n-nonadecylcyclohexane* (*cyclo* C_6C_{19}) and *octane* (C_8) in several proportions. This system was studied to obtain the wall thickness at a flow rate of 63 mL/min with the set of physical properties shown in Table 5. Results with our model including the use of the same values for C_p and k at $Re = 526$, are shown in Fig. 18, for calculations (1–4). Since the diffusion constant C_1 in Eq. (20) changes with composition, each curve was calculated with different value C_1. The layer thickness increases with time and becomes asymptotic for long times. These predictions compare well to flow data measured by Cordoba and Schall (2001) [see their Fig. 2] using the heat transfer method.

Direct comparison between predictions and experiments is shown in Fig. 19 for one specific run (calculation 3). The model under-predicts the layer thickness for short times, but agreement with experiments is good for times longer than 80 min. As discussed by Cordoba and Schall (2001),

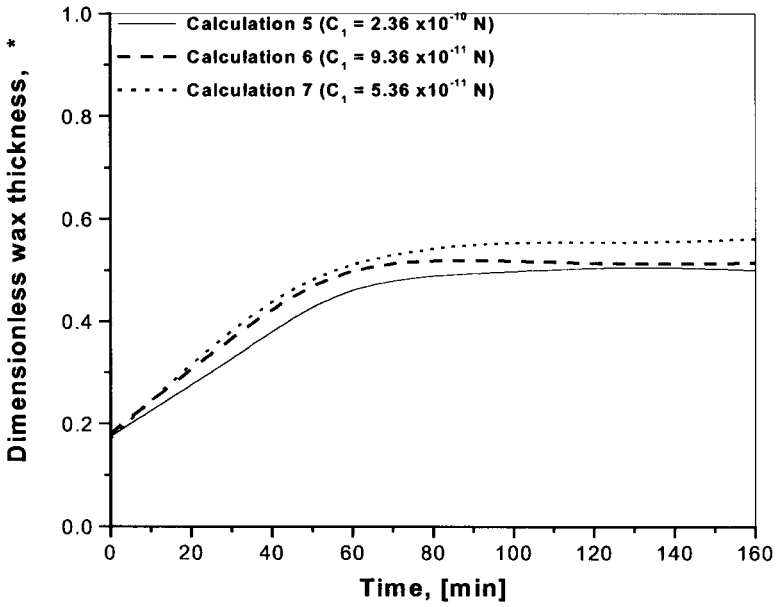

Figure 20. Present model predictions of the dimensionless wax thickness distribution vs. time for various *cyclo* C_6C_{19}:C_8 ratios given in Table 6.

the experimental results showed a deposition profile of the wax occurred very fast and randomly in the axial direction during the first minutes of the run. This resulted in unstable and nonuniform deposition at short times. Indeed, in their Fig. 4, these authors report strong fluctuations of the wax thickness at short times, where the experimental error is large. The standard deviation of wall thickness calculated from repeated experiments decreases for long times as the deposit becomes more stable and uniform. In view of the experimental uncertainties at short times, model predictions may be considered satisfactory.

In Fig. 20 we show predicted wax thickness vs. time using three different compositions (calculations 5–7, shown in Table 6), at a flow rate of 63 mL/min. According to measurements by Cordoba and Schall (2001), changes in the wax deposit composition cause a variation in normalized wall thickness of not greater than 8%.

A good agreement exists in the model predictions shown in Fig. 21 as compared to the measured values (see Fig. 3 of Cordoba and

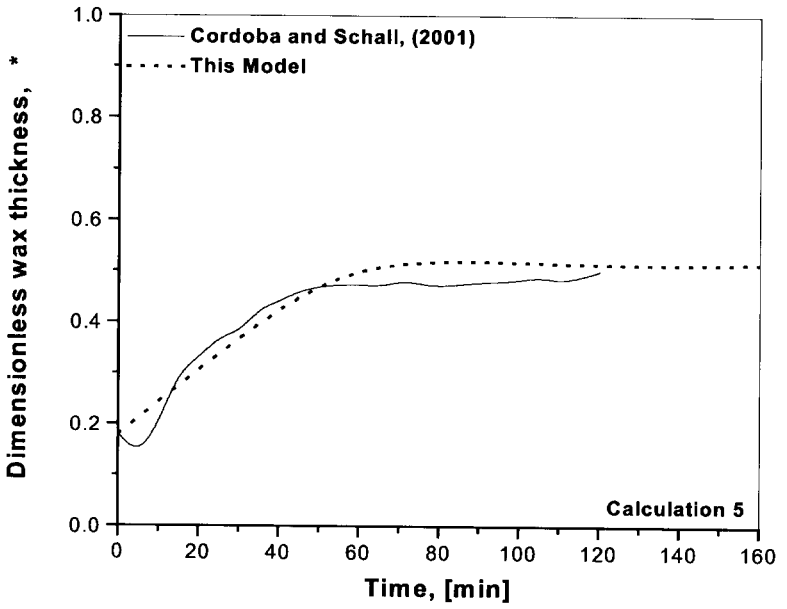

Figure 21. Dimensionless wax thickness distribution versus time. Comparison of model predictions with experimental data for the 30:70 (*cyclo* C_6C_{19}:C_8) ratio.

Table 6. Physical properties and composition for the comparison with experimental flow data.

Calculation number	Temperature (K)	C_p (J/Kg K) solution	Cyclo C_6C_{19}:C_8	k Deposit (w/mK)
1	293.15	1969	90:10	0.217
2	293.15	1969	40:60	0.161
3	303.15	2064	90:10	0.217
4	303.15	2064	40:60	0.161
5	300.65	2040.4	30:70	0.189
6	300.65	2040.4	60:40	0.189
7	300.65	2040.4	80:20	0.189

Schall (2001)). Direct comparison between predictions and experiments is shown in Fig. 21 for the 30:70 ratio (calculation 5). Once again, the model under-predicts the deposition thickness for times shorter than 30 min, but agreement is good for longer times (i.e., equilibrium times).

The asymptotic growth of layer thickness with time has been predicted by other models. Agrawal et al. (1990) and Majeed et al. (1990) also found that the deposition of normal alkanes increased asymptotically with time and reached a final and fluctuating value. This behavior is explained on the fact that a balance is reached between viscous forces and growth of the layer (Majeed et al., 1990; Wardhaugh et al., 1988). The shear forces may be significant even at low flow rates, and shear removal of deposits occurs when the wall shear stress exceeds the strength of the wall deposit. These predictions of the model are physically realistic.

CONCLUSIONS

A compositional flow model for simulating wax deposition in pipelines has been developed and tested. Results in model pipelines indicate that deposition occurs due to radial mass diffusion driven by a concentration gradient induced by a temperature gradient. The temperature distribution of the pipe in the axial and radial coordinates depends on the velocity profile which is itself a function of the rheological properties of the fluid. The mass flux for each species is a function of the thermodynamic equilibrium relations and the temperature gradient, and it strongly depends on the average diffusion constant. We have identified two parameters that profoundly influence the mass deposition rate, namely, the Reynolds number and the mass Peclet number. The contribution of flow inertia through increasing Reynolds numbers is important, as depicted in Fig. 6. No significant increases in the solid deposition are found for Reynolds numbers larger than 100. On the other hand, the effect of the mass Peclet number on the deposition amount through the average diffusion constant is very important, and strongly determines the magnitude of the radial mass flux. The concept of average diffusion constant was suggested by Burger et al. (1981) but it is known that the constant of proportionality C_1 is not easy to determine experimentally. Ribeiro et al. (1997) also assigned different values to this constant within the range explored in the present work. They also found a substantial dependence of the deposited mass layer-thickness on the value of this constant. Here, we have reached similar conclusions.

The predicted increases in the deposited layer thickness as a function of time shown in Fig. 9 illustrate that the maxima in the layer thickness occur at a specific axial location, which is defined as that where the fluid temperature reaches the cloud point. This prediction has also been verified by Elphingstone et al. (1999) in a model dealing with multiphase wax deposition. Therefore, the axial location of the onset for wax deposition is controlled by the thermodynamic equilibrium. This result derives from the fact that the thermodynamic equilibrium is reached in a time scale shorter than the characteristic time scale of the flow. The effect of the flow is clearly observed in the rate at which the mixture components are deposited (see Fig. 8).

In a multicomponent mixture in liquid–multisolid equilibrium, the thermodynamic equilibrium relations hold for only selected components (Lira-Galeana et al., 1996), thus, it is possible that different fractions might adhere to the wall at different axial locations, which in average will merge into the broad peak shown in Figs. 8 and 9.

The compositional wax deposition model proposed in Sec. 2 is compared with predictions of other models published before and with experimental flow data reported in literature. In most cases, predictions from our model are in quantitative agreement with experiments and with predictions from other models. This agreement justifies the assumptions made in the model development. A more realistic approach in which a third phase (gas phase) is considered is currently under investigation.

To summarize, among all possible identified mechanisms of wax deposition, like shear dispersion, Brownian diffusion and molecular diffusion, it is the latter the dominant mechanism (Burger et al., 1981; Elphingstone et al., 1999; Lindeloff and Krejbjerg, 2002; Ribeiro et al., 1997; Singh et al., 2000, 2001a, 2001b; Svendsen, 1993). In this work, molecular diffusion induced by a temperature gradient through the boundary layer was examined. Good agreement is found when extensive comparisons between both models and real systems are made.

ACKNOWLEDGMENTS

We thank the support of the Molecular Engineering Program of the Mexican Institute of Petroleum, grant D.00337. E. Ramirez-Jaramillo acknowledges the support from CONACyT-Mexico through grant No. 95980. Support from CONACYT through project NC-204 is also acknowledged.

NOMENCLATURE

A	Constant
B	Constant
C	Constant
C_1	Constant in average diffusion coeficient (N)
C_v	Heat capacity (J/kg K)
d	Pipe diameter (m)
D_m	Average diffusion coeficient (m^2/s)
E	Constant
F	Constant
g	Gravitational constant
$f_i(P,T,\underline{z})$	Fugacity of component i with feed composition $\underline{z}$
$f^s_{i\text{pure}}(P,T)$	Fugacity of pure solid-component i @ P and T
h_{in}	Inside convective heat transfer coefficient (W/m^2 K)
$\underline{J}$	Mass flux ($kg/s\,m^2$)
J_{MD}	Mass flux of wax due to molecular diffusion ($kg/s\,m^2$)
J_{SR}	Removal flux of wax ($kg/s\,m^2$)
J_{GD}	Mass flux of wax within the gel deposit ($kg/s\,m^2$)
k_b	Thermal conductivity of the mixture (W/m K)
k_r	Thermal conductivity of reservoir (W/m K)
k_{cem}	Thermal conductivity of cement (W/m K)
k_{an}	Thermal conductivity of material in annulus (W/m K)
k_w	Thermal conductivity of wall (W/m K)
k_s	Thermal conductivity of wax deposit (W/m K)
k_a	Thermal conductivity of acrylic cylinder (W/m K)
L	Pipe length (m)
L_s	Number of moles in solid phase
L_x	Number of moles in liquid phase
MW	Molecular weight (kg/kmol)
$M_{\text{MD}}(t,z)$	Deposited mass due to molecular diffusion (kg)
$M_{\text{SR}}(t,z)$	Removed mass due to the shear removal mechanism (kg)
$M_{\text{GD}}(t,z)$	Mass of wax molecules diffusing into the gel deposit (kg)
n	Number of components
Pe	Peclet number
ΔP	Pressure gradient
P_o	Bottom pressure (bar)
P_s	Pressure at the pipe surface (bar)
Q	Flow rate (m^3/h)
Re	Reynolds number

r_o	Inside tubing radius (m)
r_1	Outside tubing radius (m)
r_2	Inside casing radius (m)
r_3	Outside tubing radius (m)
r_4	Wellbore radius (m)
r_w	Effective radius (m)
s_i	Mole fraction in solid phase
t	Time
Δt	Time step (s)
T	Temperature (K)
T_o	Bottom temperature (K)
T_s	Temperature at the pipe surface (K)
$T_\alpha(z)$	Wall temperature along the tube (K)
U	Overall heat transfer coefficient ($W/m^2\,K$)
V	Molar volume of the mixture (m^3)
$v_z(r)$	Velocity profile (m/s)
w_s	Weight fraction of solids
w_x	Weight fraction of liquid
x_i	Mole fraction in liquid phase
$\underline{z}$	Mixture composition
z_i	Mole fraction in the mixture

Greek Letters

α	Thermal diffusivity, $\alpha = k/\rho C_p$ (m^2/s)
$\dot{\gamma}$	Shear rate (s^{-1})
η	Viscosity (Pa s)
η_b	Bulk viscosity (Pa s)
η_o	Reference viscosity (Pa s)
ρ_s	Density of solid phase (kg/m^3)
ρ_x	Density of liquid phase (kg/m^3)
ρ_m	Density of the mixture (kg/m^3)
ψ	Association parameter
$\underline{\tau}$	Shear stress tensor (Pa)
ω	Dimensionless weight function

MARCEL DEKKER, INC.
270 Madison Avenue, New York, New York 10016

APPENDIX I

Calculation Procedure

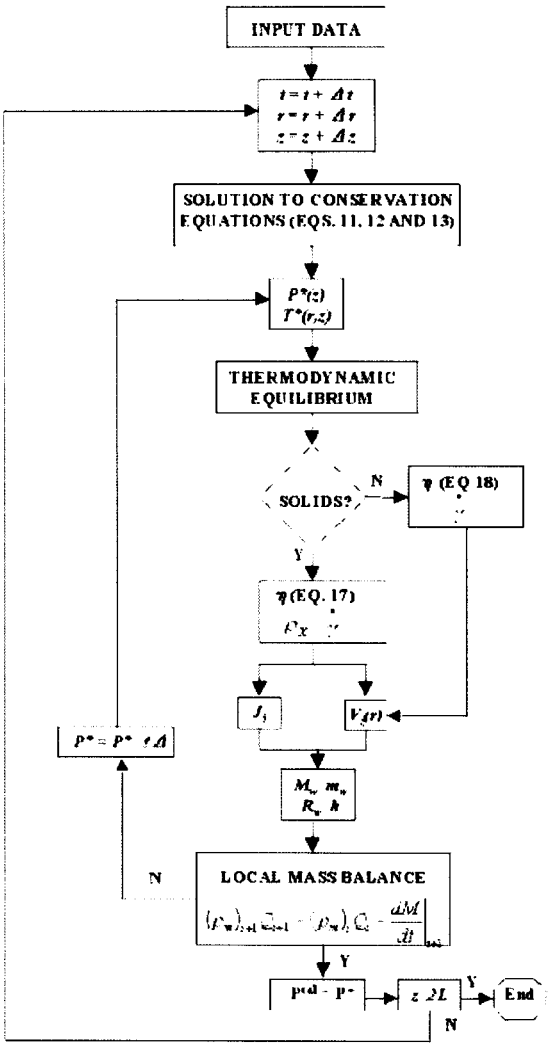

REFERENCES

Agrawal, K. M., Khan, H. U., Surianarayanan, M., Joshi, G. C. (1990). Wax deposition of Bombay high crude oil under flowing conditions. *Fuel* 69:794–796.

Burger, E. D., Perkins, T. K., Striegler, J. H. (1981). Studies of wax deposition in the trans Alaska pipeline. *J. of Petroleum Technology* 1075–1086.

Coutinho, J. A. P., Ruffier-Meeray, V. (1997). Experimental measurements and thermodynamic modeling of paraffinic wax formation in undercooled solutions. *Ind. Eng. Chem. Res.* 36:4977–4983.

Cordoba, A. J., Schall, C. A. (2001). Application of a heat method to determine wax deposition in a hydrocarbon binary mixture. *Fuel* 80:1285–1291.

Cussler, E. L., Hughes, S. E., Ward, W. J., Aris, R. (1988). Barrier membranes. *J. Memb. Sci.* 38:161.

Elphingstone, G. M., Greenhill, K. L., Hsu, J. J. C. (1999). Modelling multiphase wax deposition. *Jour. Energy Resour. Tech.* 121:81–85.

Erickson, D. D., Niesen, V. G., Brown, T. S. (1993). Thermodynamic measurement and prediction of paraffin precipitation in crude oil. In: Paper SPE 26604 in 68th Annual Conference and Exhibition of the SPE. Houston, TX, Oct. 3–6.

Goyon, J. C., Shoham, O., Brill, J. P. (1988). Analysis of computational procedures for multicomponent flow in pipelines. *SPE* 17573:219–232.

Hansen, J. H., Fredenslund, A., Pedersen, K. S., Ronningsen, H. P. (1988). A thermodynamic model for predicting wax formation in crude oils. *AIChE J.* 34(12):1937.

Hayduk, W., Minhas, B. S. (1982). Correlations for prediction of molecular diffusitivities in liquids. *Can. J. Chem. Eng.* 60:295.

Hsu, J. J. C., Santamaria, M. M. (1994). Wax deposition of waxy live crudes under turbulent flow conditions. *SPE* 28480:179–192.

Kané, M., Djabourov, M., Volle, J., Lechaire, J., Frebourg, G. (2003). Morphology of paraffin crystals in waxy crude oils cooled in quiescent conditions and under flow. *Fuel* 82:127–135.

Lindeloff, N., Andersen, S. I., Stenby, E., Heidemann, R. A. (1999). Phase-boundary calculations in systems involving more than two phases, with application to hydrocarbon mixtures. *Ind. Eng. Chem. Res.* 38(3):1107–1113.

Lindeloff, N., Krejbjerg, K. (2002). A compositional model simulating wax deposition in pipeline systems. *Energy and Fuels* 16:887–891.

MARCEL DEKKER, INC.
270 Madison Avenue, New York, New York 10016

Lira-Galeana, C., Firoozabadi, A., Prausnitz, J. M. (1996). Thermodynamics of wax precipitation in petroleum mixtures. *AIChE J.* 42(1):239.

Lira-Galeana, C., Hammam, A. (2000). Wax precipitation from petroleum fluids. A review. In: Yen, T. F., Chilingarian, R., eds. *Asphaltenes and Asphalts-II.* Chapter 21. Holland: Elsevier Science Publishers.

Majeed, A., Bringedal, B., Overa, S. (1990). Model calculates wax deposition for N Sea oils. *Oil and Gas Jour.* 18:63–69.

Nazar, A. R. S., Dabir, B., Vaziri, H., Islam, M. R. (2001). Experimental and mathematical modeling of wax deposition and propagation in pipes transporting crude oil. *SPE* 67328.

Nichita, D. V., Goual, L., Firoozabadi, A. (1999). Wax precipitation in gas condensate mixtures. In: Paper SPE 56488, in: Proceedings of the 1999 SPE Annual Technical Conference and Exhibition. Houston, TX, Oct, 3–6.

Nichita, D. V., Gomez, S., Luna, E. (2002). Phase stability analysis with cubic EOS by using a global optimization method. *Fluid Phase Equilibria* 194–197:411–437.

Pan, H., Firoozabadi, A., Fotland, P. (1997). Pressure and composition effect on wax precipitation: experimental data and model results. *SPE Production and Facilities* Nov.:250.

Pan, H., Firoozabadi, A. (1998). Complex multiphase equilibrium calculations by direct minimization of the Gibbs free energy by use of simulated annealing. *SPE Reservoir Evaluation and Engineering* Feb.:36.

Pauly, J., Daridon, J.-L., Coutinho, J. A. P., Lindeloff, N., Andersen, S. I. (2000). Prediction of solid-fluid phase diagrams of light gases-heavy paraffin systems up to 200 MPa using an EOS-GE model. *Fluid Phase Equilibria* 167:145–159.

Pedersen, K. S., Skovborg, P., Ronningsen, H. P. (1991). Wax precipipitation from north sea condensate fluids—II. Solid phase content as a function of temperature by pulsed NMR. *Energy and Fuels.* 5:924–932.

Pedersen, K. S., Ronningsen, H. P. (2000). Effect of precipitated wax on viscosity. A model for predicting non-Newtonian viscosity of crude oils. *Energy and Fuels* 14:43–51.

Ramirez-Jaramillo, E., Lira-Galeana, C., Manero, O. (2001). Numerical model for wax deposition in oil wells. *Petroleum Science and Tech.* 19(5 & 6):587–608.

Ribeiro, F. S., Souza Mendez, P. R., Braga, S. L. (1997). Obstruction of pipelines due to paraffin deposition during the flow of crude oils. *Int. J. Heat Mass Transfer* 1–10.

Singh, P., Venkatesan, R., Fogler, H. S., Nagarajan, N. (2000). Formation and aging of incipient thin film wax-oil gels. *AIChE J.* 46(5):1059–1074.

Singh, P., Venkatesan, R., Fogler, H. S., Nagarajan, N. (2001a). Morphological evolution of thick wax deposits during aging. *AIChE J.* 47(1):6–18.

Singh, P., Youyen, A., Fogler, H. S. (2001b). Existence of a critical number in the aging of a wax-oil gel. *AIChE J.* 47(9):2111–2124.

Snyder, R. G., Goh, M. C., Srivastsavoj, V. J. P., Strauss, H. L., Dorset, D. L. (1991). Kinetics of microphase demixing of short and long *n*-alkanes. *J. Phys. Chem.* 1992(96):10008.

Svendsen, J. A. (1993). Mathematical modeling of wax deposition in oil pipeline systems. *AIChE J.* 39(8):1377–1388.

Wardhaugh, L. T., Boger, D. V., Tonner, S. P. (1988). Rheology of waxy crude oils. *SPE* 17625:803–810.

Won, K. W. (1986). Thermodynamics for solid solution–liquid–vapor equilibria: wax phase formation from heavy hydrocarbon mixtures. *Fluid Phase Equilibria* 30:265.

Received January 15, 2003
Accepted May 17, 2003

MARCEL DEKKER, INC.
270 Madison Avenue, New York, New York 10016

PETROLEUM SCIENCE AND TECHNOLOGY
Vol. 22, Nos. 7 & 8, pp. 821–861, 2004

Modeling Wax Deposition in Pipelines

E. Ramirez-Jaramillo,[1] C. Lira-Galeana,[1,*] and O. Manero[2]

[1]Branch of R&D on Deep Water E&P, Mexican Institute of Petroleum, Mexico DF, Mexico
[2]Materials Research Institute, UNAM, Mexico DF, Mexico

ABSTRACT

A multicomponent liquid-wax hydrodynamic model that incorporates phase equilibria and a full non-Newtonian behavior is proposed. In this model, molecular diffusion through the boundary layer induced by a temperature gradient between the liquid and the exterior pipe wall is assumed to be the dominant mechanism for deposition. Numerical solutions to the conservation equations for Newtonian and non-Newtonian flow regimes in a model pipe are presented, and results on calculated radial mass flux and wax deposition profiles as a function of time and position in a vertical pipeline are discussed in detail. The results are compared with predictions from a previous model developed by Svendsen (Svendsen, J. A. (1993). Mathematical modeling of wax deposition

*Correspondence: C. Lira-Galeana, Molecular Engineering Research Branch, Mexican Institute of Petroleum, Av. Eje Central Lázaro Cárdenas 152, C.P. 07730, México DF, México; Fax: +52-55-3003-6239; E-mail: clira@www.imp.mx.

DOI: 10.1081/LFT-120038726
1091-6466 (Print); 821-862 (Online)

www.dekker.com